Extrusion Foaming of Semi-Crystalline PLA and PLA/Thermoplastic Starch Blends

Mihai, Mihaela; Huneault, Michel A.; Favis, Basil D.; Li, Hongbo

Publisher's version / Version de l'éditeur:
https://doi.org/10.1002/mabi.200700080
Macromolecular Bioscience, 7, 7, pp. 907-920, 2007-07-09

Extrusion Foaming of Semi-Crystalline PLA and PLA/Thermoplastic Starch Blends

Mihaela Mihai, Michel A. Huneault,* Basil D. Favis, Hongbo Li

Low density open-cell foams were obtained from polylactic acid (PLA) and from blends of PLA with thermoplastic starch (TPS) using CO_2 as a blowing agent. Two unexpected features were found. First, a 2D cavitation process in the fractured cell walls was unveiled. Elliptical cavities with dimensions in the 100–300 nm range were aligned perpendicular to large cell cracks clearly exhibiting 2D crazing prior to macroscopic cell rupture. Secondly, a significant crystallization rate increase associated with the CO_2 foaming of PLA was discovered. While the PLA used in this study crystallized very slowly in isothermal crystallization, the PLA foams exhibited up to 15% crystallinity, providing evidence that CO_2 plasticization and the biaxial stretching upon foam expansion provided conditions that could increase the crystallization rate by several orders of magnitude.

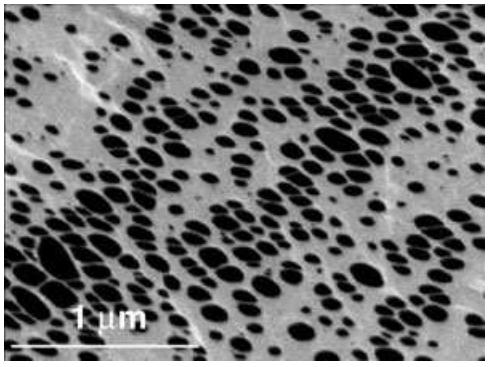

Introduction

One of the most important trends in the polymer field nowadays is the replacement of petroleum-based polymers with bio-based ones. Among bio-based polymers, polylactic acid (PLA) and thermoplastic starch (TPS) are very attractive due to their availability, relatively low cost and their appealing physical and mechanical properties. PLA is obtained on an industrial scale by the ring-opening polymerization of lactide, the cyclic dimer of lactic acid. Because lactic acid has an asymmetric carbon, C_β, the ratio between the two dimer stereoisomers, L-lactic acid and D-lactic acid, can be used to control the PLA properties and, in particular, its crystallinity. PLA obtained from a monomer feedstock comprising less than 7% D-LA (i.e., more than 93% L-lactide) will be semi-crystalline with a crystalline level that increases with monomer purity to reach around 40% for pure poly(L-lactide). Polymers obtained with more than 7% of D-LA are completely amorphous.[1,2] The crystalline level of the PLA will modulate its mechanical performance, its permeability, its heat deflection temperature and its biodegradation rate in a composting environment. PLA is a rigid and brittle polymer. The optical and mechanical properties of PLA are often compared to those of PS and PET. As a CO_2, O_2 and water vapor barrier, PLA has properties intermediate between PS and PET. With these properties, PLA has attracted growing interest as a packaging material.[2,3] However, it has lower glass transition and melt temperatures when compared to PET and PS. The lower melt temperature can be considered an advantage in terms of energy consumption during the processing step, but the lower T_g and the slow crystallization kinetics are drawbacks for many packaging applications that require a temperature resistance that exceeds the glass transition temperature, i.e., 55–57 °C. As with PET, one way

M. Mihai, B. D. Favis
CREPEC, Chemical Engineering Department, École Polytechnique de Montréal, P.O. Box 6079, Station Centre-Ville, Montréal, Québec, Canada, H3C 3A7
M. A. Huneault, H. Li
Industrial Materials Institute, National Research Council of Canada, 75 de Mortagne, Boucherville, Québec, Canada, J4B 6Y4
Fax: 1 450 641 5105; E-mail: michel.huneault@cnrc-nrc.gc.ca

DOI: 10.1002/mabi.200700080

to partially circumvent this problem is to develop a significant crystalline structure in the material during its processing. This is achieved currently in PLA by processes such as stretch blow molding and thermoforming, where the large strains imposed at relatively low temperatures are sufficient to induce PLA crystallization without hampering the material clarity. Inducing the crystallization of PLA in processes that do not involve large amounts of biaxial orientation is less trivial and is currently the subject of a lot of effort in the scientific community. It is unclear whether PLA foams with significant crystallinity can be produced and how these foams compare with current commodity packaging foams.

Because of its ability to slowly degrade in the human body, PLA was studied in biomedical applications before it gathered an appeal as a commodity resin. Therefore, it is not surprising that initial reports on PLA foaming deal mainly with a discontinuous batch foaming process for biomedical applications such as tissue engineering scaffolds. A first example is the fabrication of highly porous microcellular foams using poly[(D,L-lactic)-*co*-(glycolic acid)]. The open-cell foams were made by dissolving CO_2 into the material at elevated pressure (approximately 5.5 MPa) and then rapidly reducing the pressure to generate phase separation. The sponges created by this method had a pore size of around 100 μm. The porosity was controlled by mixing crystalline and amorphous parts and reached levels of up to 93% which corresponded to densities down to 90 $kg \cdot m^{-3}$.[4] In more recent work on batch CO_2 foaming of PLA, Fujimoto et al. (2003) showed that the foam structure could also be controlled by adding different types of clays, acting as foam nucleating agents, into semi-crystalline PLA.[5] In this case, the foam density was only reduced down to 500 $kg \cdot m^{-3}$, however. As expected for this low density reduction, the foam cells are isolated in the polymer matrix and their size is quite small, varying from 360 nm to 2.5 μm depending on the clay concentration and nature. In another report on PLA nanocomposite batch foaming, Di et al. (2004) found that nanoclays acted as foam nucleating agents.[6] In this case, the foam cells were hexagonal, indicating a much greater density reduction, and the cell size dropped from 225 μm down to around 40 μm with addition of the organoclay.

As for other polyesters, the linear molecular chain structure of PLA does not confer much elasticity in the melt state. This is inconvenient in the foaming process since melt strength is required to stabilize the foam structure prior to cooling and foam solidification. Di et al. (2005) reported chain branching of PLA in the melt state, followed by batch foaming.[7] The procedure involved first reacting a small amount of a diol (1,4-butanediol) with the PLA chain and then using a diisocyanate (1,4-butane diisocyanate) to link the chains together through the cyanate-hydroxy bonds. The modified PLA showed an enhanced melt viscosity and elasticity. The modified PLA foams, again obtained by a batch process, showed a two-fold density reduction, from 125 to 66 $kg \cdot m^{-3}$, and a six-fold cell size reduction, from 227 to 37 μm, when compared with the unmodified PLA.

One important feature of PLA, for our current purpose, is its increased crystallization rate in the presence of CO_2 at high pressures.[8] CO_2 acts as a plasticization agent, thus increasing PLA's crystallization rate and decreasing its glass transition temperature. Liao et al. (2006) indicated that small amounts of crystallites could increase the foam nucleation rate but this was possible only for a CO_2-induced crystalline fraction up to 20% in a semi-crystalline PLLA, after which the high crystalline fraction (which cannot be foamed) compromised the foam formation. In the best cases, foam densities down to around 60 $kg \cdot m^{-3}$ were obtained.[9]

Alongside PLA, thermoplastic starch is also a promising bio-based material. Starch comprises two naturally occurring polymers, namely amylose and amylopectin, that are both polysaccharides based on α-D-glucose monomeric units. The ratio between amylose and amylopectin is dependent on the starch source, but amylose is typically the minor component, accounting for around 25% of the material. Amylose is a linear macromolecule with a molar mass in the range 10^5–10^6 $g \cdot mol^{-1}$, while amylopectin is a branched one, with a larger degree of polymerization and a molecular mass of about 10^8 $g \cdot mol^{-1}$. The crystalline starch structure disappears when it is subjected to shear at temperatures greater than 70–90 °C in the presence of plasticizers such as water or glycerol. This transformation is named gelatinization and leads to so-called "thermoplastic starch" (TPS). Once the starch phase is gelatinized and properly plasticized, it can flow just as any synthetic polymer and, therefore, is suited for conventional molding and extrusion technologies. The rheological behavior and the mechanical properties of TPS can be fine-tuned with variation of the plasticizer concentration. One major drawback of TPS for most applications is its highly hygroscopic nature. To circumvent this aspect, TPS has been melt blended with a number of other polymers. The blend properties depend greatly on the composition and nature of the blended components, enabling fine-tuning of properties that could potentially suit a wide range of applications. Extensive reviews have been published on TPS blending and TPS plasticization.[10–13]

One way to foam starch is to vaporize the high water content that is comprised in humid starch. This can be achieved by a batch process known as foam baking in which the polymer ingredients are rapidly heated in a mold. Vaporization of the water expands the material up to the mold walls resulting in a molded product similar to those obtained from expanded polystyrene (PS) beads. One example of this is given in the literature for baked foams of

Macromol. Biosci. **2007**, *7*, 907–920

Macromolecular Journals
DOI: 10.1002/mabi.200700080

a blend of TPS and poly(vinyl alcohol) (PVOH).[14] Because of the inherent long cycle time, this type of process cannot be as readily and economically used for large scale production as can continuous processes such as extrusion.

Interest in the extrusion of pure starch foams first came from the food processing industry. In a report by Hutchinson et al. (1987), the mechanical properties of pure starch foams were studied as a function of the extrusion parameters and the water content used as the blowing agent.[15] A correlation between the mechanical properties of starch foams, foam density and cell wall shapes was proposed.[16] Water-foamed starch has also found uses in non-food applications, such as packaging foams known as loose fillers. Densities similar to those of the PS loose fillers can be attained. In contrast to polystyrene (PS) however, the TPS foams are compostable and their volume can be decreased by dissolving them in hot water.[17] Most applications, however, demand water insolubility. For this purpose, Fringant et al. (1996) proposed the coating of foams with a more hydrophilic material such as acetylated starch.[18] A second approach consists of foaming the acetylated starch directly instead of the pure starch.[19] Acetylated starch has reduced water solubility and is a less polar material. Other routes to decrease water solubility include the use of waxy starch (amylopectine) instead of regular starch and of course, the blending of the TPS with another less hygroscopic polymer. For foaming applications, TPS has been blended with poly[(tetramethylene adipate)-*co*-terephthalate], polycaprolactone, poly[(hydroxyl butyrate)-*co*-valerate], poly(butylenes succinate), cellulose acetate, poly(vinyl alcohol) and PLA.[20–22] The addition of 5 wt.-% to 20 wt.-% PLA was shown to improve the quality of water-foamed TPS.[21] Foam density was reduced from 62 $kg \cdot m^{-3}$ to 19 $kg \cdot m^{-3}$ upon the addition of 20 wt.-% PLA while the radial expansion ratio increased from 21 to around 44. In another study on extruded foams based on starch, up to 40 wt.-% of semi-crystalline PLA was added as a second phase. The expansion ratio was slightly improved, from 13.4 to 19.2.[22] However, this addition did not change the water solubility, the foam densities or the compressibility of foams. PLA was used with the purpose of increasing the material's elasticity, but did not lead to significant improvements in the foam's final properties.

Foaming of TPS/PLA blends in which the PLA is the matrix has not yet been reported. One reason for this may come from earlier findings reported by Martin and Averous (2001), which showed that the lack of affinity between the two polymers gave extremely coarse blend morphologies and led, in all cases, to very brittle materials.[23] Recently however, Huneault and Li (2007) reported the successful compatibilization of TPS and PLA by adding maleic anhydride (MA) grafted PLA to the blends.[24] The dispersed TPS phase size was shown to be decreased by one order of magnitude by interfacial modification while the elongation at break increased from 5–20% to the 150–250% range when different interfacial modification strategies were applied. The current work builds on these findings and evaluates the foamability of PLA/TPS blends and the effect of interfacial modification using PLA-*g*-MA. In terms of the foaming agent, water has been used in all reported TPS based foams. For most applications, water-free TPS materials will be desired, and, in the special PLA/TPS case, the presence of water as a foaming agent would result in important hydrolysis of PLA. In this context, CO_2 has been selected as a blowing agent. It is a low cost, non-flammable chemical that is highly soluble in PLA and, therefore, is a promising blowing agent for this system. The resulting foam's properties will be discussed in terms of cell morphology and density, and the crystalline content in the PLA will be analyzed using X-ray diffraction and thermal analysis.

Experimental Part

Materials

The selected PLA grade was PLA 2002D supplied by NatureWorks. It is a semi-crystalline extrusion material composed of approximately 4% of D-lactic acid monomer. It was dried at 65 °C for a minimum of 8 h prior to use. Such drying has been reported to be sufficient to decrease the moisture level to below 250 ppm and, thus, to prevent hydrolysis of PLA in the molten state. The grafting of maleic anhydride onto PLA was performed in a separate extrusion step using 2% maleic anhydride (MA) and 0.25% peroxide initiator, 2,5-dimethyl-2,5-di-(*tert*-butylperoxy)hexane or Luperox 101®, both obtained from Aldrich Chemical Company. The process configuration for the reactive extrusion step was reported previously.[24]

The wheat starch used was Supergel 1201 from ADM-Ogilvy. According to the manufacturer's data, the starch composition was 75 wt.-% amylopectine and 25 wt.-% amylose. The starch plasticizers were glycerol and water. The latter was removed during the compounding process described below, leading to a water-free TPS where glycerol was the sole plasticizer. The TPS used in the present study, after in-process moisture elimination, comprised 70 wt.-% starch and 30 wt.-% glycerol.

CO_2 with a purity of 99.9% was used as the foaming agent. The talc used as the nucleating agent was Mistron Vapor-R grade from Luzenac Corp., which had a median particle size of 2 μm and a specific surface of 13.4 $m^2 \cdot g^{-1}$. Its concentration was set to 0.5 wt.-%.

The viscosity of the investigated material was reported previously and was measured using rotational rheometry in the case of PLA and TPS/PLA blends, and by on-line capillary rheometry in the case of pure TPS and ref.[24]. Since the foaming process is highly sensitive to the materials' rheology, we reproduce in Figure 1 the main rheological features of the pure materials at 180 °C. The pure PLA exhibited a well defined Newtonian plateau typical of linear chain structures with a zero-shear

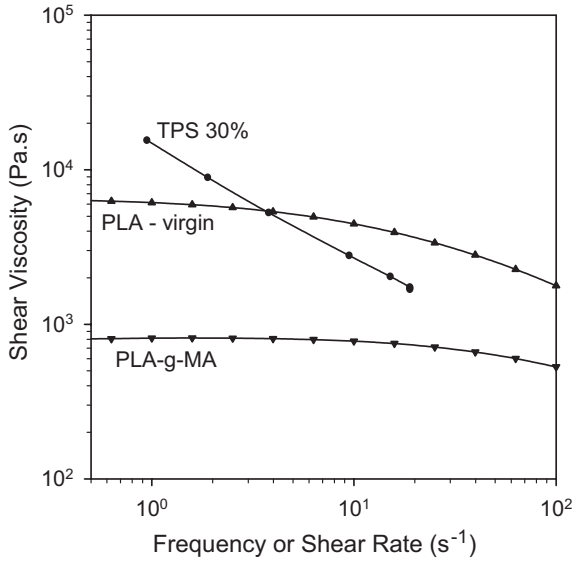

Figure 1. Viscosity of PLA, PLA-*g*-MA and TPS at 180 °C. Data for PLA is the complex viscosity as a function of frequency. Data for TPS is shear viscosity as a function of shear rate.[24]

viscosity of around 5 kPa · s^{-1}. The viscosity of the PLA-*g*- MA was significantly lower than that of the virgin PLA. It also exhibits a clearly defined Newtonian region but the zero-shear viscosity was decreased to 800 Pa · s^{-1}, a 6-fold decrease when compared to the extruded PLA control. The TPS viscous behavior is clearly very different from that of PLA. The TPS did not exhibit any viscosity plateau in the investigated shear rate range and was highly shear thinning. This is typical of branched or entangled polymer melts. Earlier work on blend rheology indicated that limited PLA hydrolysis occurred as a consequence of the blending process with TPS. Hydrolysis could be expected since the TPS necessarily comprises a higher humidity level than the dried PLA. Fortunately, this residual water is not free and thus not prone to migrate from the highly hygroscopic TPS phase to the hydrophobic PLA phase. The final blend viscosity thus remained in an acceptable range for processing.[24]

PLA/TPS Foam Extrusion

The blending procedure was based on the work of Rodriguez et al. (2003) in which the starch was fed in a slurry form to produce glycerol plasticized TPS/polyethylene blends.[25] In the current study, however, the twin-screw extrusion process had to be adapted in order to incorporate and dissolve the blowing agent into the polymer in the second half of the extruder. A sketch of the screw configuration is presented in Figure 2. The extruder was a Leistritz 34 mm co-rotating twin-screw extruder. It was operated at a screw rotation speed of 150 rpm and for a total flow rate of 10 kg · h^{-1}. A suspension made from starch/glycerol/water was fed into extruder segment 0 at a controlled rate using a volumetric slurry pump. Precise feed rate values were obtained by monitoring the loss-in-weight on the starch suspension reservoir. The first two extruder segments after feeding were used to heat and gelatinize the starch. Section 3 and 4, operated at 110 °C, were used to remove the water by atmospheric and then by vacuum vaporization, respectively, to obtain a water-free glycerol-plasticized starch. Molten PLA or PLA mixed with PLA-*g*-MA was pumped into the twin-screw segment 5 using a 25 mm single-screw extruder. The feed rate of the PLA/PLA-*g*-MA was controlled using a loss-in-weight feeder. The polymer and plasticized starch were mixed together in segment 6 and 7. The CO_2 was pumped into barrel segment 7 using a HPLC pump and the rest of the extruder length was used to solubilize the blowing agent in the polymer blend and to bring the material temperature to the desired final extrusion temperature. The screw configuration was designed to conceal the high blowing agent pressure used in the latter portion of the extruder. This was achieved by placing a pair of shear disks upstream from the blowing agent injection point. These screw elements generated a restriction to polymer flow, increasing the pressure locally, and thus creating a polymer melt seal that prevented leakage of the blowing agent upstream. A gear pump was placed at the end of the extrusion line to maintain a high pressure level in the extruder and to prevent premature bubble nucleation prior to the polymer exit from the extrusion die. In all cases, the materials were extruded through a 2 mm diameter cylindrical die. All foam samples were kept in polyethylene bags at room temperature and at 50% relative humidity prior to morphological and crystallinity characterization. All samples were dimensionally stable during that period.

CO_2 Injection Pressure Measurements

The gas injection pressure was recorded, as this is of practical importance from a technological point of view, but also because it gives a direct indication of the solubility of the blowing agent. This was achieved by measuring the gas pressure at the gas injection point in the second part of the extrusion line, i.e., into zone 7. This extruder portion was only partially filled by the polymer. Since the polymer was simply conveyed in that extruder portion, it exerted very little pressure. Therefore, the measured pressure

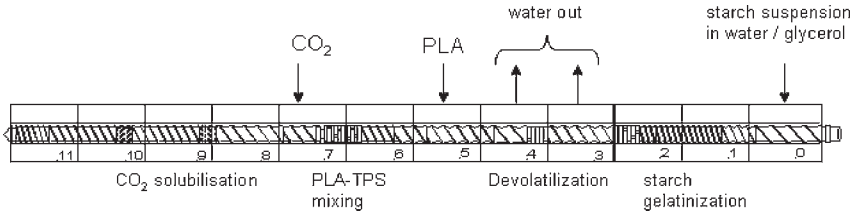

Figure 2. Twin-screw extruder configuration used to prepare the TPS/PLA blends and to incorporate the CO_2 blowing agent in a single continuous operation.

Macromol. Biosci. **2007**, *7*, 907–920

DOI: 10.1002/mabi.200700080

corresponded mainly to the pressure exerted by the blowing agent polymer solution. By definition, at steady state, the concentration of blowing agent solubilized in the polymer must equal the CO_2 concentration fed in the extruder. Since the blowing agent concentration was fixed by the operation, the only variable in the system was the blowing agent pressure, which had to adjust itself to a level that provided the required solubilization rate. Thus, the pressure-concentration data generated by this method was similar to solubility data obtained in a closed vessel using a microbalance but characterized the material in dynamic conditions. The measurements were carried out at a uniform temperature of 180 °C for all CO_2 concentrations.

Morphological Characterization

For unfoamed samples, scanning electron microscopy (SEM) was carried out on blend surfaces prepared using a microtome at −100 °C. The TPS phase was selectively extracted to enhance contrast. This was done by subjecting the sample to a 1 M HCl aqueous solution at ambient temperature for 3 h. The samples were then cleaned in a bath of demineralized water using ultrasound for 3 min. For the foamed samples, SEM observations were carried out on cryogenically fractured samples perpendicular to the extrusion direction. Selective extraction was not applied to these foamed samples. All the foamed surfaces were sputter coated with a gold/palladium alloy.

Foam Density and Open-Cell Content

The densities of the foams were determined by a water immersion method. In these measurements, at least three specimens were considered for each formulation and were cut using a razor blade at ambient temperature, since the PLA was the matrix and its glass transition temperature is around 55 °C. Open-cell fractions for the foams were determined with a Pycnometer AccuPyc 1330 from Micromeritrics using at least three specimens from each formulation. The applied pressure (N_2 gas) was set to a low value of 0.07 MPa to minimize collapse of the cellular structure and the measurements were taken after the pressure had reached an equilibrium value for 15 min. All measured values were over 60%. Since the precision of pycnometry is questionable at these high values, we refrained from using this data to compare individual samples.

Differential Scanning Calorimetry (DSC)

DSC analysis was used to evaluate the crystalline content of selected samples and to measure the isothermal crystallization rate at 100 °C. For the initial crystallization measurements, the samples were heated at 20 °C · min^{-1} and the enthalpy of crystallization upon heating ΔH_c and melting enthalpy ΔH_m were measured. The initial crystalline content in the samples is given by $(\Delta H_m - \Delta H_c)/\Delta H_f$, where ΔH_f is the theoretical heat of fusion of 100% crystalline PLA. A value of 93 J · g^{-1} was taken as PLA's theoretical heat of fusion.[31] The isothermal crystallization curves of PLA, nucleated with 1 wt.-% talc, were determined by measuring the energy released over time at a given temperature. For this purpose, the samples were heated to 200 °C in the DSC, held at that temperature for 5 min to erase the thermal history and then rapidly cooled to 100 °C. The total crystallinity developed at a given time is readily obtained by integration of the DSC heat flow curves. For the pure PLA without nucleation agent, the crystallization was so slow that the heat flow signal was below the precision range of the DSC apparatus (Perkin-Elmer, DSC-7). Therefore, the developed crystallinity could not be monitored on-line during the isothermal crystallization. The method used in this case was to anneal the samples at the crystallization temperature for a pre-determined time and then measure the sample crystallinity on a heating scan as above for the initial crystallinity evaluation. Annealing times of up to 6 h were used to monitor the crystalline growth rate of pure PLA.

X-Ray Diffraction

Wide-angle X-ray diffraction (WXRD) patterns of the foamed products were obtained with an X-ray diffractometer (D-8, Bruker). The samples were exposed to an X-ray beam with the X-ray generators running at 40 kV and 40 mA. The scanning was carried out at a rate of 0.03° · s^{-1} in the angular region (2θ) of 2–40°. The foams were compressed at room temperature using a Carver Press for 10 min to collapse the foam structure and make dense bars. Then the surfaces of the bars were carefully smoothed for XRD testing using fine sandpaper to remove any skin on the sample surface and to access the bulk of the material. As amorphous controls, bars were injection molded in a mold held at 25 °C. As fully crystallized controls, the same bars were annealed for 12 h at 100 °C.

The crystallinity fraction X_C in the samples was quantified based on the ratio of the crystalline peak area I_C over the sum of $I_C + I_A$ where I_A was the area of amorphous background for the same material. Even though this approach was less physical than integration of heat flow curves, such as in DSC, it has been shown to provide reliable information.[26] The DSC and X-ray diffraction measurements were reproduced a minimum of three times and the absolute error in the crystalline level was found to be within ±2% and ±1% respectively.

Results and Discussion

The initial blend morphology was observed on materials extruded without blowing agent. The presence of the blowing agent, because of its plasticizing effect, may induce changes in the dispersion dynamics, but the blend morphology prior to foaming gives an indication of the blend's compatibility since the dispersed phase size is directly related to the blend's interfacial tension in the melt state. Figure 3 shows only SEM micrographs for the blends comprising 33 and 50 wt.-% of TPS. In Figure 3(b) and 3(d), the PLA in the blends was substituted by a 50:50 blend of PLA and PLA-*g*-MA. Since the TPS phase was extracted prior to observation to improve contrast, it is represented by the holes (darker regions) in the micrograph. For the

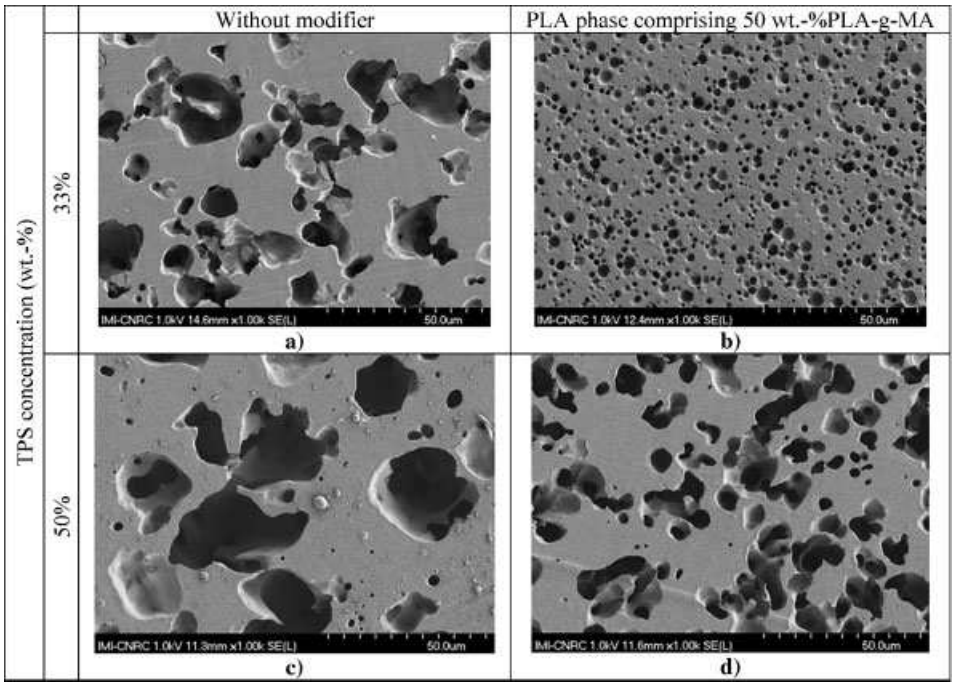

Figure 3. TPS/PLA blend morphology for blends without (left column) and with PLA-*g*-MA (right column) for TPS concentrations of 33 and 50 wt.-%.

unmodified blends, the morphology was very coarse, as expected for the uncompatibilized blend. The TPS phase presented a non-uniform size distribution with particles ranging between 5 and 20 μm for the 33 wt.-% TPS blend and between 15 and 40 μm for the 50 wt.-% TPS. The particles generally had irregular non-spherical shapes, indicating that the starch grain structure had been destroyed and that the TPS could deform freely. However, the high interfacial tension between the blend's components prevented dispersion at a finer level. In contrast, the TPS particles in the blends containing PLA-*g*-MA were much finer and more homogenously dispersed. In the 33 wt.-% TPS case, the particles were nearly spherical with diameters ranging between 1 and 5 μm. The grafted PLA, therefore, decreased the TPS phase size significantly through interfacial reactions. For the 50 wt.-% TPS blend, the TPS particles were more irregular in shape but the TPS was still the dispersed phase and no signs of co-continuity were observed.

The ability to dissolve the physical blowing agent into the polymer is of primary importance in the foaming process. For this reason, the solubility curves, i.e., the CO_2 pressure-concentration relationship, were measured in the extruder as a means to rapidly assess the solubility of CO_2 in PLA and in TPS. Figure 4 presents the CO_2 blowing agent concentration as a function of the CO_2 gas pressure measured over the gas-polymer solution at 180 °C in the closed gas pressurized portion of the extruder. As mentioned in the Experimental Part, the pressure-concentration relationship measured by this method was in principle similar to those recorded using a dedicated microbalance apparatus except that the measurement was carried out in a dynamic environment instead of a quiescent one. As expected, the CO_2 solubility increased linearly with pressure for both materials. The solubility of CO_2 was slightly higher in PLA at 0.8 wt.-%·MPa^{-1} than

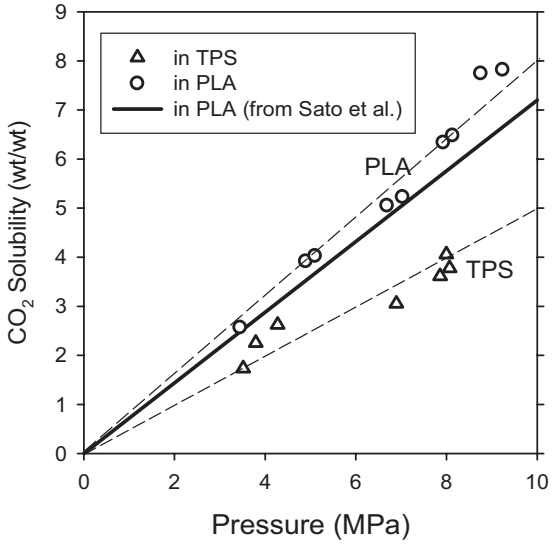

Figure 4. CO_2 solubility as a function of pressure in PLA and TPS at 180 °C. The dotted lines represent experimental data obtained from extruder in-line measurements, while the solid line is from Sato et al.[27].

Macromol. Biosci. **2007**, *7*, 907–920

DOI: 10.1002/mabi.200700080

in the TPS at around 0.5 wt.-%·MPa^{-1}. This means that the PLA phase will solubilize more CO_2 than the TPS phase for a given operating pressure. The PLA data interpolated from Sato et al. (2000) is drawn on Figure 4 for comparison.[27] Sato et al. reported solubility data obtained with a microbalance in quiescent conditions. The line shown in Figure 4 is linearly interpolated from their data at 170 °C and 190 °C. From Sato et al. data, we estimated CO_2 solubility in PLA at 180 °C of 0.72 wt.-%·MPa^{-1}. This was relatively close to the data found using the dynamic extruder data and was within the 10% accuracy limit associated with solubility measurements, even when using a sophisticated microbalance setup. Thus, we can conclude that the CO_2 was solubilized up to its equilibrium value in the dynamic extruder environment, even within the short extruder residence time.

Even though the amount of CO_2 that can be solubilized in PLA and TPS increases linearly up to elevated pressure without any apparent discontinuity, the foam fabrication experiments led to a rather surprising observation. The CO_2 incorporation into PLA or TPS/PLA blends led to very poorly expanded foams until we reached a critical CO_2 level of around 7 wt.-%, at which point the foams suddenly exhibited a high expansion ratio and a significant density reduction. Further addition of CO_2 up to around 10 wt.-% did not lead to significant density changes. Similar results were recently found in the foaming of a different PLA grade, which was totally amorphous due to a higher D-lactic acid monomer ratio.[28] Therefore, the critical CO_2 level required for low density foaming seems to be a general feature of PLA. This behavior is described in Figure 5, which shows the foam density as a function of blowing agent concentration. In the extrusion foaming process, the solubilization of the blowing agent decreases the polymer melt viscosity. Therefore, to maintain sufficient melt strength, it is necessary to progressively decrease the process temperature as the blowing agent content is increased. In the present case, at concentrations of CO_2 between 1 to 7 wt.-%, the foams collapsed significantly regardless of the extrusion temperature, which was systematically decreased from 180 to 100 °C in an effort to find some satisfactory processing window. The density of these materials fluctuated in the 600–900 kg·m^{-3}, range indicating that the blowing agent essentially escaped from materials before foam formation. In contrast, for CO_2 concentrations between 7 and 10 wt.-% into pure PLA, PLA-*g*-MA and the 33% TPS/PLA, the foam was suddenly formed and the density dropped off to values all around 25 kg·m^{-3}. For these experiments, the final extrusion temperature was set at 100 °C as a standard condition that enabled fabrication of good quality foam and acceptable screw torque. As mentioned before, the foam extrusion process temperature could be decreased significantly compared to conventional extrusion processes due to the plasticizing effect of the blowing agent, which reduced the viscosity of the polymer. The optimal foaming temperature is generally a compromise between sufficient fluidity for bubble growth and sufficient melt strength to stabilize the foam once it has expanded.

PLA and blends of TPS/PLA were foamed using a constant CO_2 concentration of 8 wt.-% to investigate formulation effects on foam density and morphology. Figure 6 presents foam density as a function of TPS fraction in the blend for different levels of PLA substitution by the MA grafted version. As a control, mixtures of PLA and PLA-*g*-MA were first foamed followed by blends comprising TPS, with and without the PLA-*g*-MA. Surprisingly, the PLA, PLA-*g*-MA and the 33%TPS/PLA blend all exhibited a

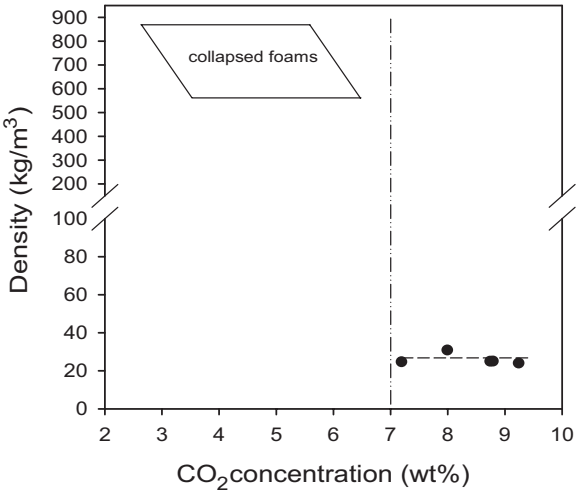

Figure 5. Variation of PLA foam density as a function of CO_2 concentration.

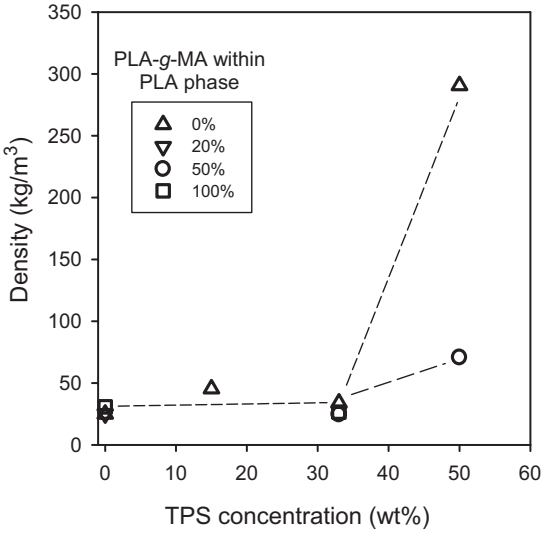

Figure 6. Foam density as a function of TPS content with various PLA-*g*-MA levels within the PLA phase. Foams produced at 100 °C using 8 wt.-% CO_2 and 0.5 wt.-% talc.

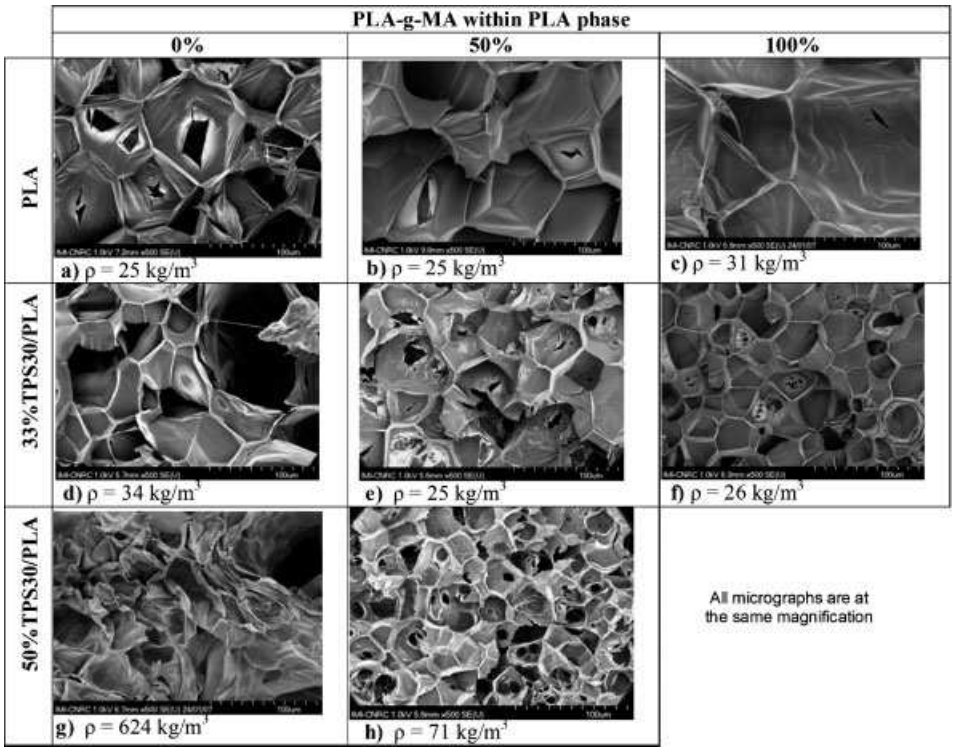

Figure 7. SEM micrographs of foam of PLA and TPS/PLA blends. The foams were produced using the same conditions as in Figure 6. Open cells (i.e., cells with broken walls) are present for all compositions.

similar density, around 25 $kg \cdot m^{-3}$, regardless of the modified PLA fraction. For the 50%TPS/PLA blend, however, the results differed dramatically depending on the grafted MA content. The non-modified blends showed a much lower density reduction than the modified ones. It is clear here that the large TPS domains observed in the microscopic analysis on the unfoamed blends were detrimental to foam formation. Microscopic observations of fractured foam surfaces were carried out to investigate the effect of blend composition on the foam morphologies and are reported in Figure 7. Figure 7(a), 7(b) and 7(c) present, respectively, the morphology of foams for unmodified PLA, a 50:50 mixture of PLA and PLA-*g*-MA, and PLA-*g*-MA. For the pure PLA foam and the 50:50 mixture, the cell dimension distributions were relatively uniform, with cell sizes between 50–100 μm. For the PLA-*g*-MA foam, the cell walls were larger and the average cell diameter exceeded 100 μm. Figure 7(d), 7(e) and 7(f) present the morphologies of the 33%TPS/PLA foams in which the PLA phase comprised, respectively, 0 wt.-%, 50 wt.-% and 100 wt.-% of the grafted PLA-*g*-MA. The addition of 33 wt.-% of TPS to PLA drastically changed the foam morphology. In the absence of modified PLA [Figure 7(d)], the foam had a bimodal morphological structure with finer cells around 30 μm and larger ones around 150–200 μm. For the foam with 50 wt.-% of PLA-*g*-MA in the PLA phase [Figure 7(e)], the cells were more uniform and finer, at around 40 μm, than in the pure PLA foams. When blending the TPS only with the PLA-*g*-MA, the foam obtained showed a further reduction in cell dimensions down to 20 μm [Figure 7(f)]. Figure 7(g), and 7(h) present the morphology of 50 wt.-%TPS/PLA foams, again with unmodified PLA and with the 50:50 mixture of PLA and grafted PLA. In this case, it is important to keep in mind that the foam density was reduced dramatically from 600 to 70 $kg \cdot m^{-3}$ upon addition of the PLA-*g*-MA. The foam of the unmodified blend showed clear signs of cell collapse while the one containing the grafted resin has a morphology that was very close to that of the 33% TPS blends.

All foams presented up to now had a high proportion of open cells. In Figure 8 and 9, higher magnification images of the foam morphologies for pure PLA and PLA/TPS blends are presented for the purpose of examining, more closely, the cell opening phenomena. The micrographs presented in Figure 8(a) show a single foam cell where one wall is ruptured. On the left part of the micrograph, is a section view of the cell walls. These are clearly less than 1 μm thick. The higher magnification micrograph of a section adjacent to the inter-cell opening [Figure 8(b)] reveals a very interesting and peculiar structure. The thin PLA wall is completely covered by extremely fine holes. These are slightly elongated in the direction of the crack and have a long axis that varied typically between 100 and 300 nm. The holes and fibrils were not randomly distributed. On the

Macromol. Biosci. **2007**, *7*, 907–920

Macromolecular Journals
DOI: 10.1002/mabi.200700080

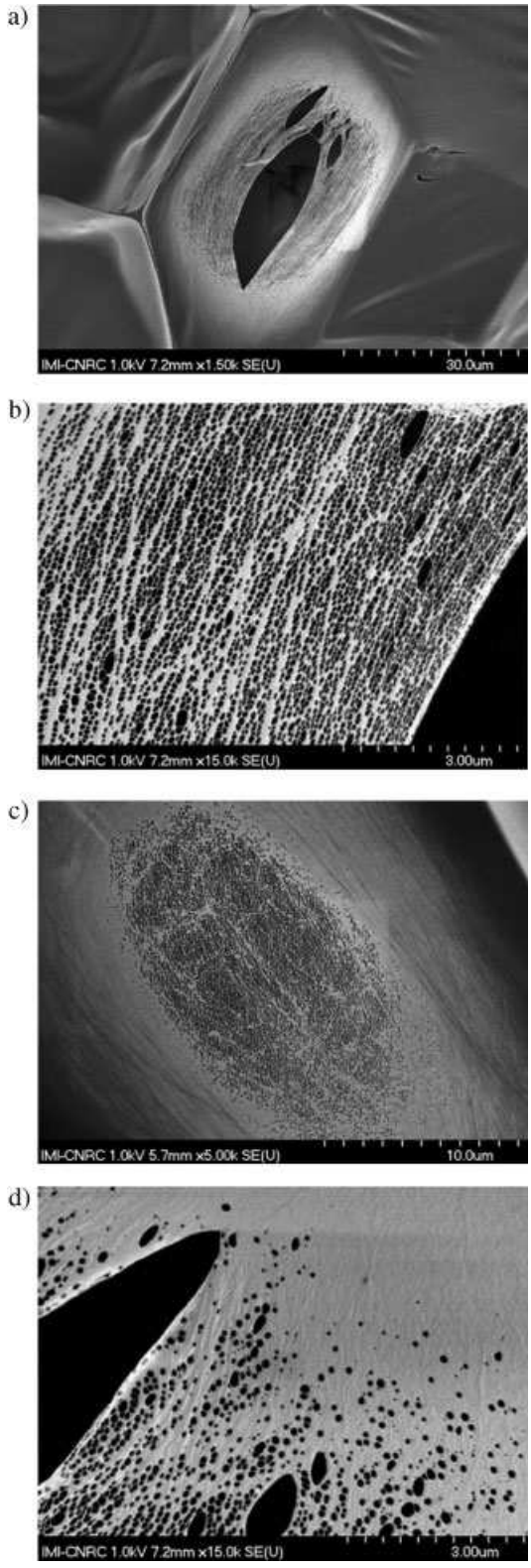

Figure 8. SEM micrographs showing (a) one ruptured cell; (b) details of the cell wall close to the crack; (c) a cavitated cell wall without rupture; (d) details near the crack end.

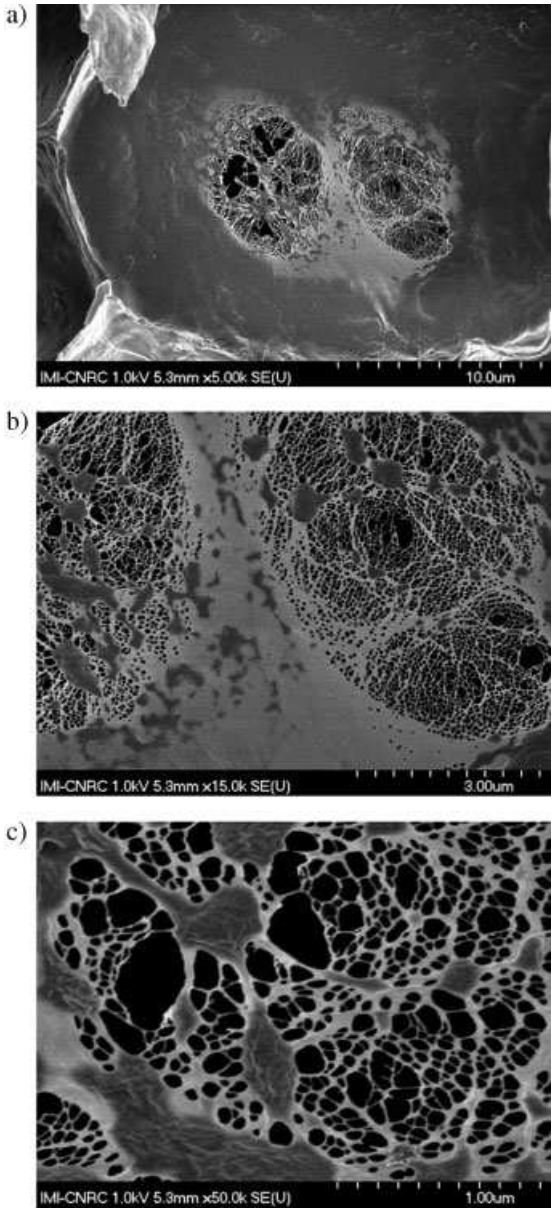

Figure 9. SEM micrographs showing: (a) one ruptured cell wall; (b)-(c) details of the cell wall opening in 50 wt.-% TPS/PLA (PLA containing 50 wt.-% PLA-*g*-MA).

contrary, the holes were preferentially arranged in lines parallel to the main cell opening and the fibrils separating these holes were in the in the direction perpendicular to the main crack. This peculiar morphology reminds us of fibrils created perpendicular to crazes (and parallel to the tensile stress direction) in glassy materials. Therefore, we can postulate that near the end of the foam cell expansion, when the cell wall thickness has been reduced to sub-micron levels, craze formation appearing perpendicular to the main stress direction is resisted by the formation of

PLA microfibrils. These morphologies are similar to the crazes observed in amorphous and semi-crystalline polymers upon deformation at temperatures below their T_g. The crazes, generally observed in 3D in thick parts, can develop in 2D (i.e., holes in a planar surface) when the film is below a critical thickness.[29] It has been postulated that crazes in semi-crystalline polymers are initiated in amorphous zones between crystal lamellae.[30] As we will discuss later, the PLA used in this study develops a crystalline structure during the foaming process. To confirm the relationship between the crystalline structure and this 2D crazing phenomenon, we carried out a similar SEM investigation on amorphous PLA foam (NatureWorks grade 8302) obtained under similar foaming conditions from another study.[28] Large holes were present in the amorphous foam cell walls but no sign of 2D crazing was found in that case. This supports the existence of a relationship between the PLA crystal structure and the 2D crazing observed.

It is interesting to reflect on the initiation and evolution of this fracture process. The foam expansion, and thus the tensile stress within cell walls, is driven by the rapid diffusion of the CO_2 dissolved in the polymer matrix to the growing foam cell. Therefore, hole and fibril formation must occur while a certain amount of CO_2 is still present in the cell walls and the pressure within the cell is sufficient to drive its expansion. The formation of the larger crack will rapidly release the blowing agent to adjacent cells, which in turn will stop the cell growth. This macrocrack formation must necessarily be catastrophic in nature since, by relieving the cell pressure, it rapidly removes the driving force of the fracture process. Thus, it can be postulated that the fracture occurs in the following steps. First, the microcraze/fibril structure is formed in a region of high stress. The holes appearing at this point are sufficiently limited in size so that the rate of CO_2 diffusion from the walls to the foam cell is greater than the gas that escapes through the porosity. Therefore, this lace structure is further stretched and thinned down to a point where a macrocrack is initiated or to a point where gas pressure has been sufficiently relieved to stop the deformation process. Note that some cell walls, with cavitation but without macrocracks, were occasionally found upon SEM examination. An example is shown in Figure 8(c). For the cell walls that underwent rupture, it can be postulated that rupture was initiated at some thinner spot or on some defect. Since the stress is maximum at the center of the cell wall, we assume the macrocrack will, most probably, be initiated near the wall center and will then propagate perpendicular to the main stress by breaking a series of successive fibrils. The crack propagates rapidly until it meets an uncavitated region, which terminates the process. This region will be more difficult to deform since it is not cavitated and stresses at this point will be smaller since this portion is closer to the cell junction (i.e., strut). This is supported by Figure 8(d) which shows the region near the end of a macrocrack. The density of holes decreases progressively as we approach the crack tip showing that the crack was terminated in a uncavitated region.

It is noteworthy that, from a macroscopic point of view, these foams did not show signs of cell collapse and exhibited high radial expansion ratios and low densities. This supports the fact that the cell wall failure mechanism was rapid and that cells were opened relatively late in the foam expansion process. The other macroscopic observation that supports the postulated mechanism is the very limited effect of blowing agent concentration in the foaming concentration range of 7–10 wt.-%. It seems that a minimum critical level is necessary to reduce PLA viscosity and to increase the thermodynamic instability required to initiate foaming, but as soon as these conditions are met, the foam expansion becomes limited by cell wall opening occurring at a certain wall stretching ratio.

It was of interest to see if this cavitation mechanism would be present in blends containing the TPS phase. A second immiscible phase could potentially act as a defect that could initiate cracks in the cell walls and promote cell opening. Figure 9 presents high magnification micrographs of a cell with an open cell wall in the case of 50 wt.-% TPS/PLA foam, in which half of the PLA phase was replaced by grafted PLA. In Figure 9(a), we see part of one foam cell surrounded on the left side of the picture by well formed struts. A ruptured region is found in the middle of the cell wall. It is different from the ruptures found in the pure PLA foams. Instead of a clear crack surrounded by small oriented holes, the wall shows a circular region where a more ductile failure occurred. Higher magnification micrographs are presented in Figure 9(b) and 9(c). The TPS phase appears as darker regions on these micrographs. The holes have appeared in the PLA phase leading to a network of very thin PLA fibrils separated by voids of uneven dimensions from 50 to 400 nm. The TPS formed larger fibrils and elongated particles with diameters between 200 nm and 1 μm. No holes were found in the darker TPS phase. It is noteworthy that the TPS phase was deformed and dispersed to a much finer level in the foaming process than in the unfoamed case [see Figure 3(d)].

Similar cavitation was found at the higher CO_2 concentrations used. However, more macroscopic changes were observed in low magnification SEM. For example, Figure 10 presents the morphology of a 33 wt.-%TPS/PLA-*g*-MA blend foamed with 10 wt.-% CO_2 comparatively to 8 wt.-% in the results presented above. The 10 wt.-% CO_2 foam exhibited similar cell sizes (25–50 μm) and a similar density (30 $kg \cdot m^{-3}$) to the one blown with 8 wt.-% CO_2. However, large cavities, up to 0.5 mm wide, were present throughout the foamed extrudates. These large cavities are

Macromol. Biosci. **2007**, *7*, 907–920

Macromolecular Journals
DOI: 10.1002/mabi.200700080

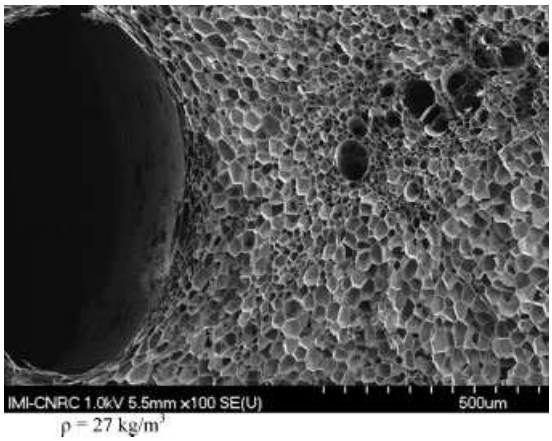

Figure 10. Low magnification SEM for the 33 wt.-% TPS/PLA-*g*-MA blend foamed with 10 wt.-% CO_2.

typically found when the blowing agent is not totally solubilized in the extrusion process and are know as blow holes to foam extrusion practitioners. Therefore, it seems that, at that concentration, the CO_2 cannot be entirely solubilized in the twin-screw mixing process. This indicates that the PLA foaming process window is relatively narrow in terms of CO_2 agent concentration.

Figure 11 presents the morphology of pure PLA foamed without talc using 8 wt.-% CO_2. This micrograph is to be compared with Figure 7(a) where 0.5 wt.-% talc was used as a nucleating agent. The foams with and without the talc show no difference in cell sizes. Furthermore, the measured foam densities were similar. This was most probably due to the high CO_2 content used in our experiments. For high blowing agent concentrations, the heterogeneous nucleation induced by talc was surpassed by the heterogeneous nucleation induced by the CO_2 concentration fluctuation. In addition, in the present extrusion foaming conditions, the CO_2 was injected in a supercritical state and could form clusters that later played the role of nucleating

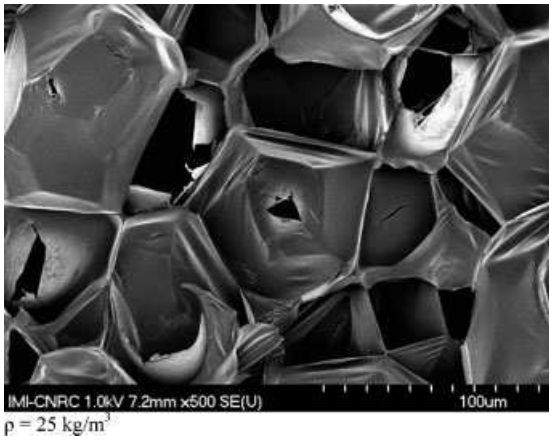

Figure 11. PLA foamed in similar conditions as in Figure 7(b), but without talc.

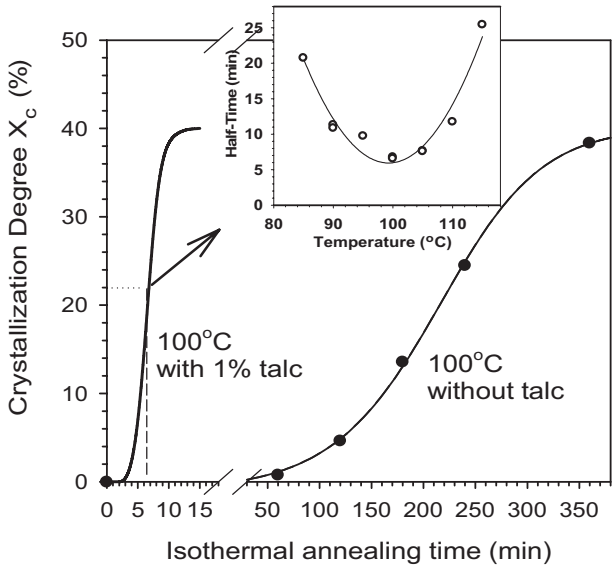

Figure 12. Crystalline fraction developed in isothermal conditions for PLA with and without talc. The half-time is the time required to reach half of the maximum crystallinity at a given temperature.

agents. It also should be noted that the whitened region around the cell wall macrocracks is a cavitated area similar to those reported in Figure 8 and 9 for foams containing 0.5 wt.-% talc. Thus, this removes any doubt concerning the potential link between the presence of talc and the observed cavitation mechanism.

Figure 12 presents the crystalline fraction development for PLA without and with 1 wt.-% talc under isothermal crystallization. As a secondary graph, the crystallization half-time as a function of temperature for PLA with talc is also included in Figure 12. The crystallization half-time is defined as the time between the start of the isothermal crystallization and the point where 50% of the ultimate crystallization fraction is completed. It can be taken as a measure of the overall rate of crystallization. The half-time curve presents a parabolic shape with an optimum crystallization temperature (i.e., half-time minimum) around 100 °C. This shape is expected from the competing effect of increased chain mobility and decreasing nucleation rate as a function of temperature. The crystalline level developed as a function of time at the optimum crystallization temperature is presented in the main graph of Figure 12. As expected, the crystalline level for PLA, with and without talc, follows a sigmoid curve to reach a plateau at around 40%. It is the timescale rather that the shape or the maximum crystallinity that is of interest here. Note that no significant crystallinity was found for pure PLA after 1 h of annealing and that it took up to 4 h to develop 20% crystallinity, which corresponds to half of the ultimate crystallinity. Thus, this PLA has a very slow crystallization rate. However, for PLA with 1 wt.-% talc, the half-time of

crystallization was shortened from hours to around 6 min. While the presence of talc did not modify the nucleation rate for the foaming process, the current data indicate that the talc can have a strong crystalline nucleation effect for PLA.

The presence of CO_2 was shown to accelerate PLA crystallization in isothermal conditions and therefore it was interesting to investigate if significant crystallinity could be achieved during the foaming process and if the talc continued to play its nucleating role in this situation.[8] Figure 13 presents a heating and cooling DSC scan of a pure PLA foam (without any talc). Upon initial heating, the T_g and enthalpic relaxation peak in the 55–60 °C area was followed by a crystallization exothermic in the 90–120 °C range and by a well defined melting endothermic. The foam initial crystalline level was given by the difference between the melting and crystallization enthalpies. Up to 15% crystallinity was found. This was a very high value considering that this crystallinity must be achieved in a few seconds rather that in hours like in the isothermal crystallization test. When the melt was cooled back after the heating run, no crystallization exothermic was observed showing that the material did not have the ability to crystallize in quiescent cooling conditions. It is clear that even though low extrusion temperatures were used, the PLA could not significantly crystallize in the extrusion process since this would rapidly increase the viscosity of the material, resulting in an abrupt stop of the extruder. Therefore, it can be postulated that the CO_2 plasticized PLA developed this significant crystallinity after exiting the die and most probably during cell growth when the cell walls were being stretched. Biaxial deformation is known to be very efficient at inducing PLA crystallization. The combination of enhanced chain mobility due to CO_2 plasticization and of strain-induced crystallization provided, in a few seconds, the same crystalline level as an isothermal annealing of more than 2 h.

To further support these findings, independent crystalline content measurements were carried out using X-ray diffraction. In DSC measurements, an incorrect baseline position can yield significant errors during the integration of the crystallization and melting peaks, especially for low crystallization rate materials. This obviously can modify the calculated crystalline level. In contrast, XRD measurements are made at room temperature and are in direct relation with the crystallinity present in the sample. Figure 14 compares the wide-angle X-ray diffraction scans for PLA and PLA/TPS foams to those of amorphous and fully crystallized PLA molded controls (see Experimental Part for control preparation). The amorphous control shows a broad "hump" while the fully crystallized PLA control presents a very strong peak at 16.40°, associated with (020) diffraction. Other typical diffraction peaks at $2\theta = 15$, 18.5 and 22.5° were also observed. The PLA foams with and without talc exhibited a significant diffraction peak at $2\theta = 16.40°$ providing further qualitative evidence of the presence of significant crystallinity in the PLA foams.

The DSC and XRD analyses were extended to PLA/TPS foams and the crystalline levels achieved in the foams are reported in Table 1. The absolute values did not coincide exactly as expected from the different probing mechanisms, but the DSC and XRD analyses both supported the fact that significant crystallinity was developed during the foaming process. It is noteworthy that, in this case, the addition of talc did not increase the crystalline level of PLA. In fact the PLA containing 0.5% talc exhibited a lower crystalline level than the pure PLA. Since the crystallization seems to be induced by the presence of the CO_2 and by the

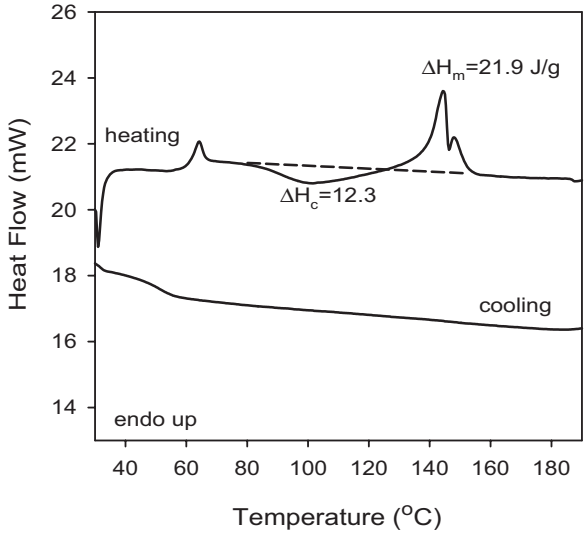

Figure 13. DSC thermogram performed on foamed PLA (without talc).

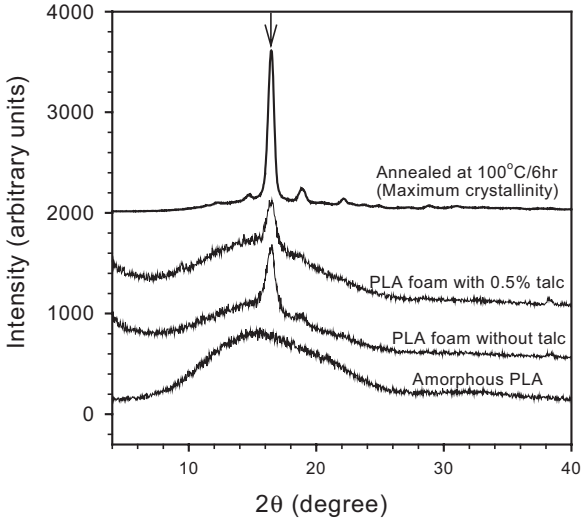

Figure 14. X-ray diffraction patterns for amorphous and crystalline PLA controls and for the PLA foams produced with and without talc.

DOI: 10.1002/mabi.200700080

Table 1. Crystallinity fraction for foamed products.

Sample	Crystalline content	
	%	
	XRD	DSC
PLA	12.8	15.5
PLA with talc	6.9	15.8
33 wt.-%TPS/PLA (50 wt.-% PLA-*g*-MA)	13.5	19.5
50 wt.-%TPS/PLA (50 wt.-% PLA-*g*-MA)	14.5	22.8
Fully crystallized control	45	42

strain during the blowing process rather than by composition heterogeneity, it may be postulated that the talc hinders the polymer chain mobility and thus decreases slightly the crystal growth rate. On the other hand, the addition of TPS had a mild positive effect on the foam's crystallinity. To the best of our knowledge, this is the first time that such a significant crystallization rate increase has been described in relation with the combined effect of plasticization and strain-induced crystallization. The close proximity of the glass transition temperature and of the optimum crystallization temperature of PLA provided particular conditions in which the blowing agent decreased significantly the viscosity, and thus increased the crystallization rate and brought the optimal crystallization temperature region into the same temperature window.

Conclusion

CO_2 is a highly soluble blowing agent for PLA (i.e., 0.8 wt.-% $\cdot$ MPa^{-1}). However, low density PLA foams were obtained only when the CO_2 concentration exceeded 7 wt.-%. The foam density decreased very suddenly at that critical CO_2 concentration and remained around 25 $kg \cdot m^{-3}$ upon further CO_2 addition. The PLA foam morphology was characterized by fine cells and high open-cell content associated with cell wall rupture during the rapid CO_2 foam cell expansion. TPS/PLA blends could also be foamed to low density values but interfacial modification using maleated PLA was necessary to obtain fine cell structures. An open-cell structure was also present when foaming these blends. Close examination of the ruptured foam cells led to the discovery of finely cavitated foam cell walls. It appeared that the semi-crystalline PLA foam wall ruptures through a sequence of events that starts with the formation of a 2D craze/fibril structure, followed by a larger scale rupture that propagates from the middle of the cell wall perpendicular to the main stretching direction. The addition of the TPS changed the ruptured cell structure leading to a less organized fibril structure and to a more ductile failure.

Another important original finding was the dramatic crystallization rate increase provided by foaming conditions. The PLA used in this study had a very slow crystallization rate with a crystallization half-time of several hours at its peak crystallization temperature of 100 °C. Surprisingly however, X-ray diffraction and differential scanning calorimetry analyses carried out on the foams indicated that significant crystallinity was developed during the foaming process. This was possible because the high CO_2 concentration highly plasticized the PLA and induced more chain mobility, which in turn accelerated the crystallization process. This finding opens the way to fabrication of PLA foams that could withstand much higher service temperatures than foams produced from amorphous PLA grades. The use of 0.5 wt.-% talc as a foam and crystalline nucleating agent did not modify the foam structure or the crystalline level achieved. For the foaming process, this indicates that the cell nucleation rate was not a limiting factor as expected from the high blowing agent concentration used. For the crystallization process, it was concluded that crystallization took place at sufficiently high undercooling such that the crystallization rate was limited by the chain mobility rather than by the nucleation rate.

Acknowledgements: The authors would like to acknowledge the financial support of *Canada's Natural Science and Engineering Research Council* and of the *Canadian Biomass Innovation Network*. The authors would also like to thank *Michel Carmel*, *François Vachon* and *Chantal Coulombe* for their technical support.

Received: March 20, 2007; Revised: May 2, 2007; Accepted: May 4, 2007; DOI: 10.1002/mabi.200700080

Keywords: foam extrusion; polylactic acid; polymer blends; thermoplastic starch

[1] D. Garlotta, *J. Polym. Environ.* **2001**, *9*, 63.
[2] R. Auras, B. Harte, S. Selke, *Macromol. Biosci.* **2004**, *4*, 835.
[3] R. Auras, S. P. Singh, J. Singh, *J. Test. Eval.* **2006**, *34*, 1.
[4] D. J. Mooney, D. F. Baldwin, N. Suh, J. P. Vacanti, R. Langre, *Biomaterials* **1996**, *17*, 1417.
[5] Y. Fujimoto, S. Sinha Ray, M. Okamoto, A. Ogami, K. Yamada, K. Ueda, *Macromol. Rapid Commun.* **2003**, *24*, 457.
[6] Y. Di, S. Iannace, E. Di Maio, L. Nicolais, *J. Polym. Sci., Part B: Polym. Phys.* **2005**, *43*, 689.
[7] Y. Di, S. Iannace, E. Di Maio, L. Nicolais, *Macromol. Mater. Eng.* **2005**, *290*, 1083.
[8] M. Takada, S. Hasegawa, M. Ohshima, *Polym. Eng. Sci.* **2004**, *44*, 186.
[9] X. Liao, A. V. Nawaby, M. Day, *PMSE Prepr.* **2006**, *95*, 613.
[10] L. Averous, *J. Macromol. Sci.* **2004**, *C44*, 231.

[11] X. L. Wang, K. K. Yang, Y. Z. Wang, *J. Macromol. Sci., Part C: Polym. Rev.* **2003**, *C43*, 385.
[12] P. Forssell, J. Mikkila, T. Suortti, *J. Macromol. Sci., Pure Appl. Chem.* **1996**, *A33*, 703.
[13] P. A. Perry, A. M. Donald, *Biomacromolecules* **2000**, *1*, 424.
[14] R. L. Shogren, J. W. Lawton, K. F. Tiefenbacher, *Ind. Crops Prod.* **2002**, *16*, 69.
[15] R. J. Hutchinson, G. D. E. Siodlak, A. C. Smith, *J. Mater. Sci.* **1987**, *22*, 3956.
[16] S. C. Warburton, A. M. Donald, A. C. Smith, *J. Mater. Sci.* **1992**, *27*, 1469.
[17] P. D. Tatarka, R. L. Cunningham, *J. Appl. Polym. Sci.* **1996**, *67*, 1157.
[18] C. Fringant, M. Rinaudo, N. Gontard, S. Guilbert, H. Darradji, *Starch* **1998**, *50*, 292.
[19] G. M. Ganjyal, N. Reddy, Y. Q. Yang, M. A. Hanna, *J. Appl. Polym. Sci.* **2004**, *93*, 2627.
[20] Q. Fang, M. A. Hanna, *Bioresour. Technol.* **2001**, *78*, 115.
[21] J. L. Willett, R. L. Shrongen, *Polymer* **2002**, *43*, 5935.
[22] Q. Fang, M. A. Hanna, *Cereal Chem.* **2002**, *77*, 779.
[23] O. Martin, L. Averous, *Polymer* **2001**, *42*, 6209.
[24] M. A. Huneault, H. Li, *Polymer* **2007**, *48*(1), 270.
[25] F. J. Rodriguez-Gonzales, B. A. Ramsay, B. D. Favis, *Polymer* **2003**, *44*, 1517.
[26] N. S. Murthy, H. Minor, *Polymer* **1990**, *31*, 996.
[27] Y. Sato, *"The 21st Japan Symposium on Thermophysical Properties"*, Nagoya 2000, p. 196.
[28] J. Reignier, R. Gendron, M. F. Champagne, *Cell. Polym.* **2007**, *26*, 83.
[29] T. Chan, A. M. Donald, E. J. Kramer, *J. Mater. Sci.* **1981**, *16*, 676.
[30] K. Friedrich, *Adv. Polym. Sci.* **1983**, *52-53*, 226.
[31] E. W. Fischer, H. J. Sterzel, G. Wegner, *Kolloid Z. Z. Polym.* **1973**, *251*, 980.

DOI: 10.1002/mabi.200700080